Charge and spin transport through a metallic ferromagnetic-paramagnetic-ferromagnetic junction

Selman Hershfield and Hui Lin Zhao*
Department of Physics and National High Magnetic Field Laboratory, University of Florida, Gainesville, Florida 32611
(Received 3 February 1997)

Using a pair of weakly coupled drift-diffusion equations for spin-up and spin-down electrons, we compute the signal of recent spin-injection experiments by Johnson on ferromagnetic-paramagnetic-ferromagnetic films. In the limit of large junction resistance, our results coincide with those of earlier calculations. As the junction resistance decreases, there are correction terms which provide a cutoff to the size of the signal for films much thinner than the spin-diffusion length. The physical origin of this cutoff is the leakage of nonequilibrium magnetization out of the paramagnet into the current and voltage probes. Although our calculation can explain the sample thickness dependence of the experiments, it cannot account for the large magnitude of the signal observed. [S0163-1829(97)03530-3]

I. INTRODUCTION

The transport of spin-polarized electrons in metals has been a subject of investigation for many years. One way to generate spin-polarized electrons is to drive a current from a ferromagnetic metal to a nonmagnetic material. The earliest tunneling experiment done in this context was by Tedrow and Meservey, who drove a current from a ferromagnetic film to a superconductor.[1] An alternative method is to create a tunnel junction with a spin-dependent transmission probability or resistance. For example, such a junction can be created using a magnetic semiconductor for the barrier between two normal metals.[2] Of course, in any real experiment involving current flow from a ferromagnet to a paramagnet, the nonequilibrium magnetization is due to both the polarization of the electrons in the ferromagnet and the spin-dependent transmission probabilities at the interface.

In recent years, one phenomena involving polarized electrons which has attracted a great deal of experimental[3,4] and theoretical[5,6] interest is the giant magnetoresistance seen in magnetic multilayers. In these experiments the resistivity of alternating layers of magnetic and nonmagnetic metals depends crucially on whether the magnetizations of adjacent magnetic layers are parallel or antiparallel. Since the layers can be aligned with small fields, one can see large changes in the resistance with small applied magnetic fields, leading to technological applications as well as raising fundamental physics questions.[7]

In this paper we consider a different but not unrelated set of experiments called spin-injection experiments developed by Johnson and Silsbee over the last 10 years.[8,9] With this technique a nonequilibrium population of spin-polarized electrons is created by driving a current from a ferromagnet to a paramagnet[10] and then detected with the use of a second ferromagnet.[11] In Fig. 1 we show the geometry of Johnson's most recent spin-injection experiment.[12] A current is driven from the ferromagnetic metal labeled F1 to the paramagnetic metal labeled P. This creates a nonequilibrium magnetization which extends roughly one spin-diffusion length into the paramagnet. One way to think of a nonequilibrium magnetization is that spin-up and spin-down electrons have different chemical potentials. The clever part of this and the earlier spin-injection experiments is to measure the chemical potential difference between the two spin species using a second ferromagnetic voltage probe, shown as F2 in Fig. 1.

In thin magnetic films such as those used in the experiment the magnetization tends to be parallel to the plane of the film. By applying a sufficiently large magnetic field parallel to the film, the magnetization of the two ferromagnetic films can be aligned parallel to one another. Since the films will in general not have the same coercivities, as one reduces and then reverses the direction of the magnetic field, at some point the magnetization of one of the films will flip before the other. At this point the ferromagnets F1 and F2 will have antiparallel magnetizations. Continuing to increase the magnitude of the magnetic field, the other film will reverse its direction of magnetization and the two films will again have parallel magnetizations.

What is measured experimentally is the voltage of the

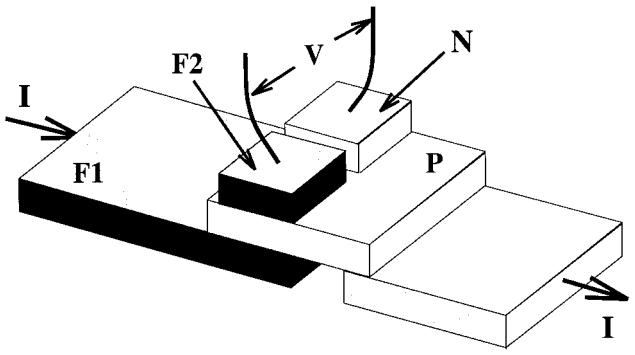

FIG. 1. The experimental geometry of the spin-injection experiment of Ref. 12. Current flows from the ferromagnetic current probe F1 to the paramagnet P creating a nonequilibrium magnetization in P. The voltage is measured between the ferromagnetic voltage probe F2 and the paramagnetic voltage probe N. This is done both for parallel alignment of the magnetizations of the two ferromagnetic films (V_I) and for antiparallel alignment of the magnetizations (V_{II}). The difference $V_I - V_{II}$ divided by the current I is the signal R_S.

ferromagnetic voltage probe F2 relative to a reference paramagnetic metal voltage probe, N. When F1 and F2 have parallel magnetizations, one voltage is measured, which we will denote as V_I. When the magnetizations are antiparallel, another voltage is measured, V_{II}. The voltage difference $V_I - V_{II}$ divided by the electrical current injected, I, is defined as R_S

$$R_S = (V_I - V_{II})/I, \tag{1.1}$$

which is the spin-injection signal.

To see that the voltage difference $V_I - V_{II}$ and R_S are related to the difference in the chemical potentials for spin-up and spin-down electrons, we consider the limiting case discussed in Ref. 8 when only one of the spin species, $s = \uparrow$, is occupied in the ferromagnets. When the ferromagnetic voltage probe is placed in contact with the paramagnet, the chemical potential of F2 will align with the chemical potential $\mu_\uparrow$ for the spin-up electrons in P at the interface. If we flip the direction of magnetization of F2 so that only the $s = \downarrow$ electrons are occupied, then the chemical potential in the ferromagnetic voltage probe will align with the spin-down chemical potential $\mu_\downarrow$ in P at the interface. Thus, by measuring the difference between the chemical potentials of F2 for these two cases, using a paramagnetic voltage probe, N, as a reference, one can directly measure $\mu_\uparrow - \mu_\downarrow$. For the case when only one spin species is occupied, $-e(V_I - V_{II})$ is identically equal to $(\mu_\uparrow - \mu_\downarrow)$. For an experiment using a ferromagnetic material like iron or Permalloy, the ferromagnet will have nonzero occupation of both spin species and $-e(V_I - V_{II})$ will be proportional to $(\mu_\uparrow - \mu_\downarrow)$.

Johnson and Silsbee have performed both thermodynamic and microscopic analyses of their spin-injection experiment.[9] When applied to the experiment shown in Fig. 1 one finds that for thicknesses d of the paramagnetic film (P) less than the spin-diffusion length in the paramagnet δ_S, the signal grows as $1/d$:

$$R_S \approx \eta_1 \eta_2 \frac{\rho \delta_S^2}{2\mathcal{A}d}, \tag{1.2}$$

while in the opposite limit where $d \gg \delta_S$, the signal decays exponentially

$$R_S \approx \eta_1 \eta_2 \frac{\rho \delta_S}{\mathcal{A}} e^{-d/\delta_S}. \tag{1.3}$$

In both Eqs. (1.2) and (1.3) the resistivity of the paramagnetic film is ρ, the cross-sectional area of the current probe is $\mathcal{A}$, and the factors η_1 and η_2 are dimensionless parameters. The first dimensionless parameter η_1 is the polarization of the current at the F1-P interface,

$$\eta_1 = \frac{I_\uparrow - I_\downarrow}{I_\uparrow + I_\downarrow}, \tag{1.4}$$

where I_s is the electrical current carried by spin-up $(s = \uparrow)$ and spin-down $(s = \downarrow)$ electrons. For the case in which only one spin species carries current η_1 is equal to one. The second dimensionless parameter is a measure of how closely the ferromagnetic voltage probe measures the difference in the chemical potentials for spin-up and spin-down electrons in the paramagnet

$$\eta_2 = \frac{-e(V_I - V_{II})}{\mu_\uparrow - \mu_\downarrow}. \tag{1.5}$$

As discussed above, one would expect $\eta_2 = 1$ for a ferromagnet with only one spin species occupied.

One of the most interesting features of the experiment in Ref. 12 is that the resistance R_S does indeed grow like $1/d$ for $d < \delta_S$. Thus, this is an effect which increases as sample sizes are made smaller, which is highly desirable for technological considerations. Another interesting and unexpected feature of the experiment is that the product $\eta_1 \eta_2$ appears to be larger than one, which is counterintuitive.

To better understand both the small thickness behavior and the size of $\eta_1 \eta_2$, in this paper we present another analysis of the spin-injection experiment based on a two-component drift-diffusion equation, one component for each spin. One could also use higher component drift-diffusion equations or the full Boltzmann equation; however, since even with a simple two-component model we cannot determine all the parameters, we feel that a more sophisticated analysis is not justified at this point. The approach used here is related to both the microscopic approach used by Johnson and Silsbee[9] and recent theory of the perpendicular magnetoresistance in magnetic multilayers by Johnson[13] and by Valet and Fert.[14] In particular the work of Valet and Fert also uses spatially-dependent chemical potentials and boundary conditions at the interface similar to ours. They have also recently analyzed Johnon's experiment.[15]

Our goal in this paper is to answer the following questions: At the microscopic level of this model, what determines η_1 and η_2? Can either η_1 or η_2 be larger than unity? As the sample thickness is made smaller, does the signal diverge as $1/d$ or is there a cutoff? If there is a cutoff, what governs the scale of it? In the end we will reproduce the results of Johnson and Silsbee in the limit of large junction resistance between the ferromagnets and the paramagnet. As the resistance is decreased, however, there are corrections. Some of these corrections may be important already in the present experiments.

The rest of this paper is organized as follows. In the next section we introduce our two-component drift-diffusion equation, solve it in a bulk system, and introduce the spin and charge modes. In Sec. III we treat the case of one junction between a ferromagnet and a paramagnet. This is actually a calculation of the parameter η_1. By working through this case in detail, we are able to simplify the treatment of the full ferromagnet-paramagnet-ferromagnet junction described in Sec. IV. In Sec. IV we also argue that this three-terminal geometry is sufficient to explain the experiment of Ref. 12. Thus, in Sec. V we compare the results of our calculation to the experiment. All the results are summarized in Sec. VI. An appendix gives an alternate derivation of the results in Sec. IV and V based on the Onsager relations for resistance measurements.

II. CHARGE AND SPIN MODES

The model used consists of spin-up and spin-down electrons which diffuse independently except for weak scattering from one spin to the other. The two kinds of electrons, $s = \uparrow$ or $\downarrow$, have different diffusion constants, D_s, density of

states, $N_s(E_F)$, and conductivities, $\sigma_s = e^2 N_s(E_F) D_s$. The current densities $\mathbf{j}_s$ for spin-up and spin-down electrons are determined by the electric field $\mathbf{E}$ and the density n_s:

$$\mathbf{j}_\uparrow = \sigma_\uparrow \mathbf{E} - D_\uparrow \nabla n_\uparrow , \tag{2.1}$$

$$\mathbf{j}_\downarrow = \sigma_\downarrow \mathbf{E} - D_\downarrow \nabla n_\downarrow . \tag{2.2}$$

The electric field is in turn determined by Gauss's Law,

$$\nabla \cdot \mathbf{E} = \frac{1}{\epsilon_0}(n_\uparrow + n_\downarrow). \tag{2.3}$$

The rate at which spin-up electrons scatter to spin-down electrons is denoted by $1/\tau_{\uparrow\downarrow}$. Likewise, spin-down electrons scatter to spin-up electrons with rate, $1/\tau_{\downarrow\uparrow}$. In steady state this scattering can be included via

$$\nabla \cdot \mathbf{j}_\uparrow = -\frac{n_\uparrow}{\tau_{\uparrow\downarrow}} + \frac{n_\downarrow}{\tau_{\downarrow\uparrow}}, \tag{2.4}$$

$$\nabla \cdot \mathbf{j}_\downarrow = -\frac{n_\downarrow}{\tau_{\downarrow\uparrow}} + \frac{n_\uparrow}{\tau_{\uparrow\downarrow}}. \tag{2.5}$$

Equations (2.1)–(2.5) are the basic equations which we solve. They satisfy current conservation because the sum of Eq. (2.4) and Eq. (2.5) is zero: $\nabla \cdot (\mathbf{j}_\uparrow + \mathbf{j}_\downarrow) = 0$. They can also be combined to form the drift-diffusion equation by taking the divergence of Eqs. (2.1) and (2.2) and substituting in Eqs. (2.3)–(2.5):

$$\nabla^2 \begin{pmatrix} n_\uparrow \\ n_\downarrow \end{pmatrix} = \begin{pmatrix} \kappa_\uparrow^2 + \dfrac{1}{D_\uparrow \tau_{\uparrow\downarrow}} & \kappa_\uparrow^2 - \dfrac{1}{D_\uparrow \tau_{\downarrow\uparrow}} \\ \kappa_\downarrow^2 - \dfrac{1}{D_\downarrow \tau_{\uparrow\downarrow}} & \kappa_\downarrow^2 + \dfrac{1}{D_\downarrow \tau_{\downarrow\uparrow}} \end{pmatrix} \begin{pmatrix} n_\uparrow \\ n_\downarrow \end{pmatrix}, \tag{2.6}$$

where

$$\kappa_s^2 = \sigma_s / (D_s \epsilon_0) = e^2 N_s(E_F)/\epsilon_0 , \tag{2.7}$$

and κ_s is the inverse of the screening length, which is by far the smallest length scale in the problem.

We first examine the case when the spin-up and spin-down electrons are not coupled, i.e., $1/\tau_{\uparrow\downarrow} = 1/\tau_{\downarrow\uparrow} = 0$. In this case the matrix on the right-hand side of Eq. (2.6) is easily diagonalized. We will call the two eigenvectors the spin and charge modes and label them as v_S and v_Q. The eigenvalues have units of inverse length squared so we denote them by $(\lambda_S)^2$ and $(\lambda_Q)^2$, where λ has units of inverse length. With these conventions the eigenvectors and eigenvalues are

$$v_Q = \begin{pmatrix} \gamma_\uparrow \\ \gamma_\downarrow \end{pmatrix}, \quad (\lambda_Q)^2 = \kappa_\uparrow^2 + \kappa_\downarrow^2 , \tag{2.8}$$

$$v_S = \begin{pmatrix} 1 \\ -1 \end{pmatrix}, \quad (\lambda_S)^2 = 0, \tag{2.9}$$

where γ_s is the fraction of the density of states at the Fermi surface due to spin-up and spin-down electrons:

$$\gamma_s = \frac{N_s(E_F)}{N_s(E_F) + N_{-s}(E_F)}. \tag{2.10}$$

From Eqs. (2.8) and (2.9) we can see much of the basic physics. First, in this no-coupling limit, the spin mode has no net charge density. It is truly a spin mode. Also, in the no-coupling limit the spin mode does not decay in space, $\lambda_S = 0$. Since the charge mode's divergence is zero and it decays in space, the charge mode does not carry any current. Thus, in the no-coupling limit the spin mode has no net charge and does not decay, and the charge mode carries no current.

The two scattering lifetimes, $\tau_{\uparrow\downarrow}$ and $\tau_{\downarrow\uparrow}$, can also be related using the above equations. The net rate of scattering of up electrons to down electrons is given by the right-hand side of Eq. (2.4). Similarly, the net rate of scattering of down electrons to up electrons is given by the right-hand side of Eq. (2.5). If we uniformly shift the chemical potential of the entire system, then this rate should not change, and consequently

$$\frac{N_\uparrow(E_F)}{\tau_{\uparrow\downarrow}} - \frac{N_\downarrow(E_F)}{\tau_{\downarrow\uparrow}} = 0. \tag{2.11}$$

This equation can also be justified by the Boltzmann equation.

With a finite, but weak, coupling between spin-up and spin-down electrons, the spin-mode carries a small amount of charge and decays over a long length scale, the spin diffusion length. To see this, we expand the eigenvectors and eigenvalues of the matrix in Eq. (2.6) to lowest order in the ratio of the κ_s^{-2} to the $D_{s'}\tau_{s'',-s''}$ in Eq. (2.6). The κ_s^{-1} are of the order of the (charge) screening length, while the $(D_{s'}\tau_{s'',-s''})^{-1/2}$ are of the order of the spin-diffusion length. Since the screening length is of the order of an Angstrom and the spin-diffusion length is of the order of 100 Å or larger, this is a good approximation. The resulting eigenvectors and eigenvalues for the spin mode are

$$v_S = \begin{pmatrix} 1 + \alpha/2 \\ -1 + \alpha/2 \end{pmatrix}, \quad (\lambda_S)^2 = \left(\frac{\gamma_\downarrow}{D_\uparrow} + \frac{\gamma_\uparrow}{D_\downarrow} \right) \frac{1}{\tau_S}, \tag{2.12}$$

where the spin-relaxation rate is

$$\frac{1}{\tau_S} = \frac{1}{\tau_{\uparrow\downarrow}} + \frac{1}{\tau_{\downarrow\uparrow}}, \tag{2.13}$$

and the dimensionless factor α is

$$\alpha = \frac{1}{\kappa_\uparrow^2 + \kappa_\downarrow^2} \left(\frac{1}{D_\downarrow} - \frac{1}{D_\uparrow} \right) \frac{1}{\tau_S}. \tag{2.14}$$

Thus, if we allow electrons to scatter from one spin to the other, the spin mode has a finite but long decay length (spin-diffusion length), and it has a finite but small charge density. Because of the relation Eq. (2.11), the eigenvector of the charge mode remains the same. The eigenvalue does change, but the change is small and can be neglected. This is different from the spin mode, where the spin-coupling correction could not be neglected because both the charge carried by the spin mode and λ_S^{-1} are zero without spin coupling.

In actually matching boundary conditions and solving the drift-diffusion equation, it is more convenient to work with the spin-dependent electrochemical potential, $\mu_s(\mathbf{x})$, than the

density, $n_s(\mathbf{x})$, of Eq. (2.6). The spin-dependent electrochemical potential is defined by

$$n_s(\mathbf{x}) = -eN_s(E_F)[\mu_s(\mathbf{x}) + eV(\mathbf{x})] \tag{2.15}$$

or equivalently by

$$\frac{\mu_s(\mathbf{x})}{-e} = V(\mathbf{x}) + \frac{n_s(\mathbf{x})}{e^2 N_s(E_F)}, \tag{2.16}$$

where $V(\mathbf{x})$ is the electrical potential, $\mathbf{E} = -\nabla V(\mathbf{x})$. From Eqs. (2.1) and (2.2) the electrochemical potential is simply related to the current via

$$\mathbf{j}_s = -\sigma_s \nabla\left(\frac{\mu_s}{-e}\right). \tag{2.17}$$

Although both the density, $n(\mathbf{x})$, and the electrical potential, $V(\mathbf{x})$, vary over a charge screening length near a boundary, the electrochemical potential defined in Eq. (2.16) is smooth over a charge screening length. This can be readily seen by computing the equation for the electrochemical potentials from Eqs. (2.1)–(2.6):

$$\nabla^2\begin{pmatrix}\mu_\uparrow\\ \mu_\downarrow\end{pmatrix} = \begin{pmatrix} +\dfrac{1}{D_\uparrow\tau_{\uparrow\downarrow}} & -\dfrac{1}{D_\uparrow\tau_{\uparrow\downarrow}} \\ -\dfrac{1}{D_\downarrow\tau_{\downarrow\uparrow}} & +\dfrac{1}{D_\downarrow\tau_{\downarrow\uparrow}}\end{pmatrix}\begin{pmatrix}\mu_\uparrow\\ \mu_\downarrow\end{pmatrix}. \tag{2.18}$$

The matrix in Eq. (2.18) has two eigenvalues and eigenvectors, which again correspond to the charge and spin modes. Because the electrochemical potential is a linear combination of the excess charge density n_s and the electrical potential V, the eigenvectors are changed. The new charge mode eigenvector and eigenvalue are

$$v'_Q = \begin{pmatrix}1\\ 1\end{pmatrix}, \quad (\lambda'_Q)^2 = 0. \tag{2.19}$$

The fact that the charge eigenvalue is zero does not mean that there is no screening, but only that the electrochemical potential does not vary over a charge screening length. The new spin mode eigenvector and eigenvalue are

$$v'_S = \frac{1}{\sigma_\uparrow + \sigma_\downarrow}\begin{pmatrix}\sigma_\downarrow\\ -\sigma_\uparrow\end{pmatrix}, \quad (\lambda'_S)^2 = (\lambda_S)^2. \tag{2.20}$$

The electrochemical potential varies over the same spin-diffusion length as the density.

The reason that the electrochemical potential is more useful than the density in solving this problem is that it varies over only one length scale, the spin-diffusion length, which is much larger than a mean free path. We can expect a diffusion equation to describe behavior on length scales large compared to a mean free path, but not behavior on length scales much smaller than the mean free path, e.g., the charge screening length. Furthermore, we will see in the next section that the difference in the electrochemical potential is what enters into our Landauer formula boundary condition describing the current across a boundary between two materials.

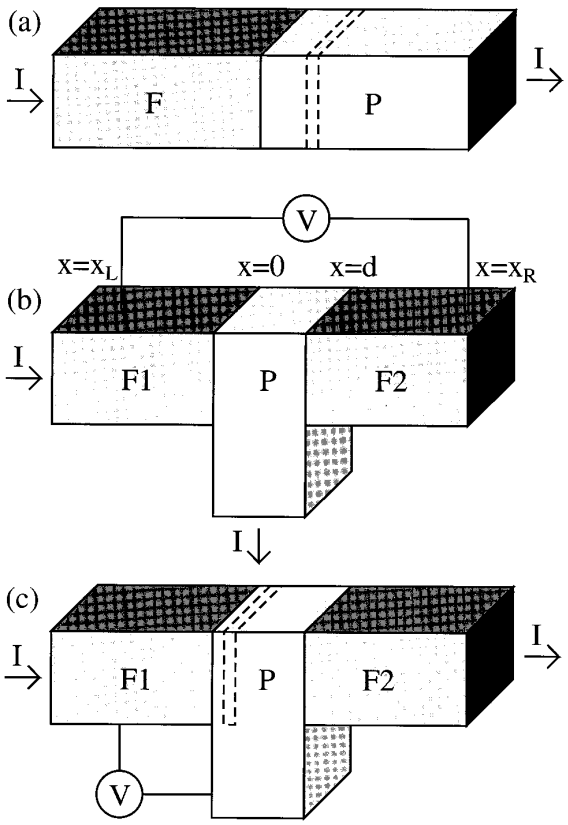

FIG. 2. Idealized two-terminal and three-terminal spin-injection geometries. (a) In the two-terminal geometry used in Sec. III current flows from the ferromagnet F to the paramagnet P. (b) In the three-terminal geometry used in Sec. IV current enters through the ferromagnetic current probe F1 and exits through the paramagnetic current probe P. The ferromagnetic voltage probe F2, is used to measure the nonequilibrium magnetization in P. (c) In the three-terminal geometry used in the Appendix current enters through F1 and exits through F2. The voltage V measured in (b) and (c) is the same because of the Onsager relations for a resistance measurement. The dashed lines indicate a typical slab used to reduce the three-dimensional problem to an effective one-dimensional problem via the divergence theorem.

III. ONE JUNCTION

Before going to the three-terminal case we first consider the simpler two-terminal geometry shown in Fig. 2(a). Although this case has been treated by a number of authors, we go through it in detail because it will allow us to introduce the basic boundary conditions used in the more complicated three-terminal geometry and hence simplify the more difficult case.

As a first step we reduce the three-dimensional equations to one-dimensional equations. A set of one-dimensional functions are defined by integrating their three-dimensional counterparts over a cross-sectional area $\mathcal{A}$:

$$\mu(x) = \frac{1}{\mathcal{A}}\int d^2x_\perp \mu(\mathbf{x}), \tag{3.1}$$

$$j(x) = \frac{1}{\mathcal{A}}\int d^2x_\perp (\mathbf{j}(\mathbf{x}))_x. \tag{3.2}$$

The x direction is the direction of current flow as shown in Fig. 2(a). If one assumes that there is no current flowing out the sides of the wire, then applying the divergence theorem to a slab like the one in Fig. 2(a) allows one to reduce Eq. (2.18) to a one-dimensional equation:

$$\frac{d^2}{dx^2}\begin{pmatrix}\mu_\uparrow\\ \mu_\downarrow\end{pmatrix}=\begin{pmatrix}+\dfrac{1}{D_\uparrow\tau_{\uparrow\downarrow}} & -\dfrac{1}{D_\uparrow\tau_{\uparrow\downarrow}}\\ -\dfrac{1}{D_\downarrow\tau_{\downarrow\uparrow}} & +\dfrac{1}{D_\downarrow\tau_{\downarrow\uparrow}}\end{pmatrix}\begin{pmatrix}\mu_\uparrow\\ \mu_\downarrow\end{pmatrix}. \tag{3.3}$$

The current in the x direction is also given by a one-dimensional equation

$$j_s(x)=-\sigma_s\frac{d\mu_s(x)/(-e)}{dx}. \tag{3.4}$$

Equations (3.3) and (3.4) are satisfied on both the left-hand side (ferromagnet, F) and right-hand side (paramagnet, P) of the junction. We denote the different values of the screening lengths, conductivities, etc., on the two sides of the junction with superscripts L and R. Using the eigenvalues and eigenvectors of Eqs. (2.19) and (2.20), the solution of Eq. (3.3) on the left-hand side ($x<0$) has the form

$$\frac{1}{j}\begin{pmatrix}\mu_\uparrow/(-e)\\ \mu_\downarrow/(-e)\end{pmatrix}=(A^Lx+B^L)\begin{pmatrix}1\\1\end{pmatrix}+\frac{j^L}{2\lambda_S^L}e^{+\lambda_S^Lx}\begin{pmatrix}+(\sigma_\uparrow^L)^{-1}\\ -(\sigma_\downarrow^L)^{-1}\end{pmatrix}. \tag{3.5}$$

In Eq. (3.5) we have explicitly divided out the net current density, j, which is the sum of the spin-up and spin-down current densities. The net current density is constant because of current conservation. The solution is determined from three constants, A^L, B^L, and j^L, which will be determined by matching boundary conditions at the interface between the two regions. The solution on the right-hand side ($x>0$) has a similar form and also contains three unknowns, which we denote as A^R, B^R, and j^R:

$$\frac{1}{j}\begin{pmatrix}\mu_\uparrow/(-e)\\ \mu_\downarrow/(-e)\end{pmatrix}=(A^Rx+B^R)\begin{pmatrix}1\\1\end{pmatrix}+\frac{j^R}{2\lambda_S^R}e^{-\lambda_S^Rx}\begin{pmatrix}+(\sigma_\uparrow^R)^{-1}\\ -(\sigma_\downarrow^R)^{-1}\end{pmatrix}. \tag{3.6}$$

Equations (3.5) and (3.6) have a total of six unknowns. Far away from the junction, the electrochemical potentials for spin-up and spin-down electrons are the same. There is an arbitrary offset in defining the electrochemical potential. This offset can be fixed by one of the variables, say B^L. This leaves five remaining unknowns, which are solved via five boundary conditions. Below we examine these boundary conditions one at a time.

1,2. The net current at $x=+\infty$ is the same as the net current at $x=-\infty$ and equal to j. The electrical current is related to the electrochemical potential via Eq. (3.4). Since the spin modes decay, the currents at $\pm\infty$ are entirely determined by the electric fields at $\pm\infty$: $j=(\sigma_\uparrow+\sigma_\downarrow)E$. Taking the derivative of the electrochemical potentials in Eqs. (3.5) and (3.6), this boundary condition determines the coefficients A^L and A^R:

$$A^L=\frac{-1}{\sigma_\uparrow^L+\sigma_\downarrow^L}, \tag{3.7}$$

$$A^R=\frac{-1}{\sigma_\uparrow^R+\sigma_\downarrow^R}. \tag{3.8}$$

3. The spin current is continuous across the interface. Spin-flip scattering could be included; however, this would tend to reduce the spin polarization, since it allows the magnetization to relax. Because we are interested in seeing how large the effect can be theoretically, we do not include spin-flip scattering. Again using Eq. (3.4) to compute the current, the spin current boundary condition yields

$$\frac{\sigma_\uparrow^L-\sigma_\downarrow^L}{\sigma_\uparrow^L+\sigma_\downarrow^L}-j^L=j^R. \tag{3.9}$$

4, 5. The current across the junction is determined by the difference in the electrochemical potential across the junction. Up to this point we have not said anything about the transparency or opacity of the interface between the two regions. Using a Landauer formula[16] the current is determined by the difference in the electrochemical potential on the left side and right side of the junction, $\mu_s(0^-)$ and $\mu_s(0^+)$, respectively. Letting the conductances per unit area for spin-up and spin-down electrons be $G_\uparrow$ and $G_\downarrow$, the spin-up and spin-down currents are

$$j_\uparrow(0)=G_\uparrow\left(\frac{\mu_\uparrow(0^-)}{-e}-\frac{\mu_\uparrow(0^+)}{-e}\right), \tag{3.10}$$

$$j_\downarrow(0)=G_\downarrow\left(\frac{\mu_\downarrow(0^-)}{-e}-\frac{\mu_\downarrow(0^+)}{-e}\right). \tag{3.11}$$

Before solving Eqs. (3.7)–(3.11) we introduce some notation which will simplify the equations. We let the polarization of the current far to the left of the junction be defined as p,

$$p=\frac{\sigma_\uparrow^L-\sigma_\downarrow^L}{\sigma_\uparrow^L+\sigma_\downarrow^L}. \tag{3.12}$$

For this junction, there is no polarization far to the right of the junction because the right-hand side is a paramagnet. As described in the introduction, we define the spin polarization at the interface to be η_1 [see Eq. (1.4)]. The voltage drop across the interface due to the charge mode is defined as V:

$$V=B^L-B^R. \tag{3.13}$$

Finally, we introduce two quantities which have the dimensions of resistance per unit area:

$$R_s^L=\frac{1}{\sigma_s^L\lambda_S^L}, \tag{3.14}$$

$$R_s^R=\frac{1}{\sigma_s^R\lambda_S^R}. \tag{3.15}$$

They are the resistance per unit area of a region one spin-diffusion length long. Consequently, a longer spin-diffusion length means a larger R^L or R^R.

With these definitions, the now three equations which must be solved are

$$\eta_1 = p^L - j^L = j^R, \tag{3.16}$$

$$\frac{1+\eta_1}{2} = G_\uparrow\left\{\frac{V}{j} + \frac{R^L_\uparrow j^L}{2} - \frac{R^R_\uparrow j^R}{2}\right\}, \tag{3.17}$$

$$\frac{1-\eta_1}{2} = G_\downarrow\left\{\frac{V}{j} - \frac{R^L_\downarrow j^L}{2} + \frac{R^R_\downarrow j^R}{2}\right\}. \tag{3.18}$$

The solution for η_1 from these equations is

$$\eta_1 = \frac{1/G_\downarrow - 1/G_\uparrow + p^L(R^L_\downarrow + R^L_\uparrow)}{1/G_\downarrow + 1/G_\uparrow + R^L_\downarrow + R^L_\uparrow + R^R_\downarrow + R^R_\uparrow}. \tag{3.19}$$

There are several limits of Eq. (3.19) which can be easily understood. First if the junction has a large resistance, $1/G_s \gg R^L_s$, R^R_s, then the expression for η_1 of Johnson and Silsbee is reproduced exactly.[9] Second, if the spin relaxation in the leads is weak, i.e., R^L_s, $R^R_s \gg 1/G_s$, then η_1 is determined by the polarization p of the electrons coming from the ferromagnet. In the intermediate regime, Eq. (3.19) interpolates between the two limits. Note that in no case is η_1 of Eq. (3.19) larger than one.

IV. THREE-TERMINAL DEVICE

There are two important observations to make to reduce the actual experimental geometry shown in Fig. 1 to a three-terminal geometry. First, the voltage probes are perpendicular to the electrical current flow. Consequently, there is no Ohmic voltage drop between the two voltage probes. Second, the length scale of the cross-sectional area of the voltage probes is much larger than the spin-diffusion length. Thus, the leakage of the nonequilibrium magnetization from the region under one voltage probe to the other is negligible. We can regard the two voltage probes independently. Instead of working with a four-terminal geometry, we can use the three-terminal geometry shown in Fig. 2(b). Since the voltage between the paramagnet P and the paramagnetic voltage probe N is independent of the relative orientation of the ferromagnets, the experimentally relevant voltage is the voltage of the ferromagnetic voltage probe relative to some reference voltage. Remember, the signal is determined by the difference between the voltage when the ferromagnets have parallel magnetizations, V_I, minus the voltage when they have antiparallel magnetizations, V_{II}. We will take as our reference voltage a point far into the left lead, $x_L \ll 0$, where the electrochemical potentials for spin-up and spin-down electrons are equal. The voltage at this point is taken to be zero: $0 = \mu_\uparrow(x_L) = \mu_\downarrow(x_L)$.

The actual current flows in Fig. 2(b) are complex because the current must change direction as it goes from the ferromagnet F1 to the paramagnet P. None the less one can derive effective one-dimensional equations. In this section we present a derivation similar to the one used in the previous section. In the Appendix we present another derivation of the same result based on the Onsager relations for resistance measurements.

As in Sec. III, we apply the divergence theorem to a thin slab. In the ferromagnetic regions, F1 and F2, the integrals over the sides of the wire vanish because no current flows out the sides. Thus, one-dimensional equations can be derived for $x<0$,

$$\frac{1}{j}\begin{pmatrix}\mu_\uparrow/(-e)\\ \mu_\downarrow/(-e)\end{pmatrix} = \frac{-(x-x_L)}{\sigma^L_\uparrow+\sigma^L_\downarrow}\begin{pmatrix}1\\1\end{pmatrix} + \frac{j^L}{2\lambda^L_S}e^{+\lambda^L_S x}\begin{pmatrix}+(\sigma^L_\uparrow)^{-1}\\ -(\sigma^L_\downarrow)^{-1}\end{pmatrix}, \tag{4.1}$$

and for $x>d$

$$\frac{1}{j}\begin{pmatrix}\mu_\uparrow/(-e)\\ \mu_\downarrow/(-e)\end{pmatrix} = B^R\begin{pmatrix}1\\1\end{pmatrix} + \frac{j^R}{2\lambda^R_S}e^{-\lambda^R_S(x-d)}\begin{pmatrix}+(\sigma^R_\uparrow)^{-1}\\ -(\sigma^R_\downarrow)^{-1}\end{pmatrix}. \tag{4.2}$$

In Eq. (4.1) the boundary condition that the net incoming current density is j has been included by setting the coefficient of x for the charge mode equal to $-1/(\sigma^L_\uparrow+\sigma^L_\downarrow)$. Similarly, the fact there is no net current going into the voltage probe has been included by taking the coefficient of x in Eq. (4.2) to be zero.

The situation is more complicated in the paramagnetic region P, where the lower edge of the slab is not on a boundary [see Fig. 2(b)]. At this boundary, $j_s = -\sigma_s \nabla \mu_s$ is definitely not zero because the current exits there. The key here is to look at the spin current instead of the charge current. By subtracting the spin-up and spin-down electrochemical potentials in Eq. (2.18), we obtain

$$\nabla^2[\mu_\uparrow(\mathbf{x}) - \mu_\downarrow(\mathbf{x})] = \frac{1}{D\tau_S}[\mu_\uparrow(\mathbf{x}) - \mu_\downarrow(\mathbf{x})], \tag{4.3}$$

where $D = D_\uparrow = D_\downarrow$ is the diffusion constant in the paramagnet. There is a leakage of the spin current, $-\sigma^M(\mu_\uparrow - \mu_\downarrow)$, out the lower boundary; however, the reduction of the nonequilibrium magnetization due to this spin current is small compared to the decay due to spin-flip scattering (τ_S) because the size of the voltage pads is much larger than the spin-diffusion length. In Johnson's experiment, the voltage pads have an area of 10^{-2} mm^2, which is large compared to spin-diffusion length, which is at most of order a micron. This means that even though $\nabla(\mu_\uparrow - \mu_\downarrow)$ is not zero at the lower boundary, it is small, and one can derive a one-dimensional equation for the difference in the electrochemical potentials in the paramagnet:

$$\frac{d^2[\mu_\uparrow(x) - \mu_\downarrow(x)]}{dx^2} = \frac{1}{D\tau_S}[\mu_\uparrow(x) - \mu_\downarrow(x)]. \tag{4.4}$$

This equation has a solution of the form ($0<x<d$):

$$\frac{\mu_\uparrow(x) - \mu_\downarrow(x)}{(-e)j} = \left(\frac{1}{\sigma^M_\uparrow} + \frac{1}{\sigma^M_\downarrow}\right)\left\{\frac{j^{M1}}{2\lambda^M_S}e^{-\lambda^M_S x} + \frac{j^{M2}}{2\lambda^M_S}e^{\lambda^M_S(x-d)}\right\}. \tag{4.5}$$

We now match boundary conditions between the two regions as in the previous section. The conditions for continuity of the spin current at $x=0$ and $x=d$ are

$$p-j^L=j^{M1}-j^{M2}e^{-\lambda_S^M d}, \tag{4.6}$$

$$j^R=j^{M1}e^{-\lambda_S^M d}-j^{M2}, \tag{4.7}$$

where p is defined in Eq. (3.12). The other important boundary conditions are the Landauer formula boundary conditions like Eqs. (3.10) and (3.11). Equation (4.5) allows us to relate the difference in the electrochemical potentials between spin-up and spin-down electrons at $x=0$ and at $x=d$, but it does not relate the average electrochemical potential between the two sides. Fortunately, the Landauer formula boundary condition only involves the difference in the electrochemical potential between points $x=0^-$ and $x=0^+$ and between the points $x=d^-$ and $x=d^+$. The part of the voltage drop at the interface due to the charge mode [V in Eq. (3.13)] can be treated as an unknown. In analogy with Eq. (3.13) we define V^L to be the voltage drop at $x=0$ due to the charge mode and V^R to be corresponding the voltage drop at $x=d$. The four equations for the two junctions with two possible spin orientations is then

$$1+p-j^L=G_\uparrow^L\left(\frac{2V^L}{j}+R_\uparrow^L j^L-R_\uparrow^M[j^{M1}+j^{M2}e^{-\lambda_S^M d}]\right), \tag{4.8}$$

$$1-p+j^L=G_\downarrow^L\left(\frac{2V^L}{j}-R_\downarrow^L j^L+R_\downarrow^M[j^{M1}+j^{M2}e^{-\lambda_S^M d}]\right), \tag{4.9}$$

$$j^R=G_\uparrow^R\left(\frac{2V^R}{j}+R_\uparrow^M[j^{M1}e^{-\lambda_S^M d}+j^{M2}]-R_\uparrow^R j^R\right), \tag{4.10}$$

$$-j^R=G_\downarrow^R\left(\frac{2V^R}{j}-R_\downarrow^M[j^{M1}e^{-\lambda_S^M d}+j^{M2}]+R_\downarrow^R j^R\right). \tag{4.11}$$

The factors of 2 appear in these equations because we have multiplied by 2 on both sides of the equations [see Eqs. (3.17) and (3.18)]. The resistances R_s are defined as in Eqs. (3.14) and (3.15). The six equations, Eqs. (4.6)–(4.11), are the equations which must be solved in order to compute the signal measured in the experiment. In the next section we discuss the results of the solution.

V. RESULTS

The voltage V measured in Fig. 2(b) is measured relative to the x_L. In terms of the electrochemical potentials it is given by

$$V=\left(\frac{\mu_s(x_R)}{-e}\right)-\left(\frac{\mu_s(x_L)}{-e}\right), \tag{5.1}$$

where s is $\uparrow$ or $\downarrow$. Implicit in Eq. (5.1) is that the ends of the voltage probes are further than a spin-diffusion length away from the interfaces at $x=0$ and $x=d$ so that the electrochemical potentials for spin-up and spin-down electrons are the same. The signal measured is the difference of the voltage, V, shown in Fig. 2(b) for F1 and F2 with parallel magnetizations (configuration I) minus the voltage measured for F1 and F2 with antiparallel magnetizations (configuration II).

$$R_S=\left(\frac{V}{j\mathcal{A}}\right)_I-\left(\frac{V}{j\mathcal{A}}\right)_{II}. \tag{5.2}$$

To go from configuration I to configuration II in Eq. (5.2) one interchanges the spin-up and spin-down parameters, σ_s, D_s, G_s, ... in one of the ferromagnets. This corresponds to flipping the magnetization in that ferromagnet.

The voltage V is the sum of several different contributions. There are voltage drops in going from $x=x_L$ to $x=0^-$, from $x=0^-$ to $x=0^+$, from $x=0^+$ to $x=d^-$, from $x=d^-$ to $x=d^+$, and from $x=d^+$ to $x=x_R$. These terms may be computed using Eqs. (4.1), (4.2), and (4.5), as well as the definitions of V^L and V^R used in computing the drop across the interface in Eqs. (4.8)–(4.11). The result is

$$V=-\frac{|x_L|}{\sigma_\uparrow^L+\sigma_\downarrow^L}-V^L+\left(\frac{\mu_\uparrow(d^-)+\mu_\downarrow(d^-)}{2(-e)}-\frac{\mu_\uparrow(0^+)+\mu_\downarrow(0^+)}{2(-e)}\right)-V^R. \tag{5.3}$$

The first term in Eq. (5.3) is invariant upon changing the direction of the magnetizations in either ferromagnet. Consequently, it drops out of the difference in Eq. (5.2). Upon solving for V^L, one finds that it is also unchanged after reversing the magnetization direction in one of the ferromagnets. The third term in Eq. (5.3) is the voltage drop in the paramagnet due to the charge current flow. It is not associated with the nonequilibrium magnetization because it is the average of the electrochemical potentials for spin-up and spin-down electrons. One would thus expect it to also be independent of the orientation of the ferromagnets. Unfortunately, within this approach we cannot compute it directly; however, by comparison to the Onsager relation approach described in the Appendix we will see that this term is indeed invariant under magnetization reversal. We are left with only the last term V^R as contributing to the signal R_S:

$$R_S=\left(\frac{-V^R}{j\mathcal{A}}\right)_I-\left(\frac{-V^R}{j\mathcal{A}}\right)_{II}. \tag{5.4}$$

In order to write the signal R_S in as simple a manner as possible we introduce two dimensionless quantities η_1' and η_2', which will reduce precisely to the η_1 and η_2 expressions of Johnson in some limiting cases.

$$\eta_1'=\frac{1/G_\downarrow^L-1/G_\uparrow^L+p(R_\uparrow^L+R_\downarrow^L)}{1/G_\downarrow^L+1/G_\uparrow^L+R_\uparrow^L+R_\downarrow^L}, \tag{5.5}$$

$$\eta_2'=\frac{1/G_\downarrow^R-1/G_\uparrow^R+R_\downarrow^R-R_\uparrow^R}{1/G_\downarrow^R+1/G_\uparrow^R+R_\uparrow^R+R_\downarrow^R}. \tag{5.6}$$

In these equations and all subsequent equations the parameters, $G_\downarrow$, $G_\uparrow$, $R_\downarrow$, and $R_\uparrow$, are those in the parallel magnetization configuration (configuration I). We also introduce two dimensionless ratios of resistances, r_L and r_R, which

compare the junction resistance $1/G_s$ to the resistance associated with the spin diffusion in the leads R_s:

$$r_L=\frac{1/G_{\downarrow}^{L}+1/G_{\uparrow}^{L}+R_{\uparrow}^{L}+R_{\downarrow}^{L}}{R_{\uparrow}^{M}+R_{\downarrow}^{M}}, \tag{5.7}$$

$$r_R=\frac{1/G_{\downarrow}^{R}+1/G_{\uparrow}^{R}+R_{\uparrow}^{R}+R_{\downarrow}^{R}}{R_{\uparrow}^{M}+R_{\downarrow}^{M}}. \tag{5.8}$$

With these definitions, the result for R_S is

$$R_S=\frac{1}{2}\eta_1'\eta_2'\frac{R_{\uparrow}^{M}+R_{\downarrow}^{M}}{\mathcal{A}}\left\{\cosh\left(\frac{d}{\delta_S}\right)\left(\frac{1}{r_L}+\frac{1}{r_R}\right)+\sinh\left(\frac{d}{\delta_S}\right)\left(1+\frac{1}{r_L r_R}\right)\right\}^{-1}, \tag{5.9}$$

where δ_S is the spin-diffusion length in the paramagnet. In the notation of the previous section $\delta_S=(\lambda_S^M)^{-1}$. Below we examine several limiting cases of this equation for R_S.

When the junction resistance is large compared to the resistance associated with spin diffusion, the dimensionless ratios r_L and r_R are much larger than one. In this limit we recover the Johnson and Silsbee[9] result for η_1 and η_2:

$$\eta_1'\rightarrow\frac{G_{\uparrow}^{L}-G_{\downarrow}^{L}}{G_{\uparrow}^{L}+G_{\downarrow}^{L}}, \tag{5.10}$$

$$\eta_2'\rightarrow\frac{G_{\uparrow}^{R}-G_{\downarrow}^{R}}{G_{\uparrow}^{R}+G_{\downarrow}^{R}}. \tag{5.11}$$

Provided that d/δ_S is not too small, the resistance R_S also reduces in this limit to

$$R_S\approx\frac{1}{2}\eta_1'\eta_2'\frac{R_{\uparrow}^{M}+R_{\downarrow}^{M}}{\mathcal{A}}\frac{1}{\sinh(d/\delta_S)}. \tag{5.12}$$

This is again in agreement with Johnson's results [see Eqs. (1.2) and (1.3)]. One of the most interesting features of Eq. (5.12) is that the signal R_S becomes larger as the sample becomes smaller. Indeed for $d\ll\delta_S$, the signal diverges as $R_S\sim 1/d$. This is clearly not physical. The full result, Eq. (5.9), does not diverge for very thin samples, but rather approaches

$$R_S\rightarrow\frac{1}{2}\eta_1'\eta_2'\frac{R_{\uparrow}^{M}+R_{\downarrow}^{M}}{\mathcal{A}}\left\{\frac{1}{r_L}+\frac{1}{r_R}\right\}^{-1}. \tag{5.13}$$

The origin of the divergence in Eq. (5.12) is that we have effectively taken the resistance of the junction to be infinitely large (compared to R_s). If we keep the current fixed, then the magnetization density is proportional to $I\tau_S/\mathcal{A}d$. In reality, though, this density will not become infinite, but some of the magnetization will leak out into the ferromagnetic current or voltage probes. The length at which this happens is set by the dimensionless ratios r_L and r_R.

In Fig. 3 we have plotted R_S as a function of d/δ_S for different values of $r=r_L=r_R$. The product $\eta_1'\eta_2'$ is set equal to one, which is the largest possible value of the product. As expected, all the curves decay exponentially for $d>\delta_S$. The $d<\delta_S$ behavior is different for the three values of r. For large junction resistance ($r=100$) the product $R_S d$ is roughly constant for a wide range of $d<\delta_S$, while for smaller junction resistances ($r=10$ or $r=1$), $R_S d$ decays more rapidly. Even for large junction resistance, $R_S d$ does eventually decay for small d. The points are from the experiment of Ref. 12 for the case where Permalloy is the ferromagnet. In plotting the data we have used two different values for the spin-diffusion length: $\delta_S=1\ \mu$m (squares) and $\delta_S=4\ \mu$m (circles). As explained in Ref. 12 if one adjusts δ_S to fit the falloff at large d, then the signal is larger than the theory, and if one adjusts δ_S to fit the small d data, then the experiment decays more quickly than the theory at large d. The resistivity of the paramagnet P is ρ, and $\mathcal{A}$ is the cross-sectional area of the current probe in Fig. 2.

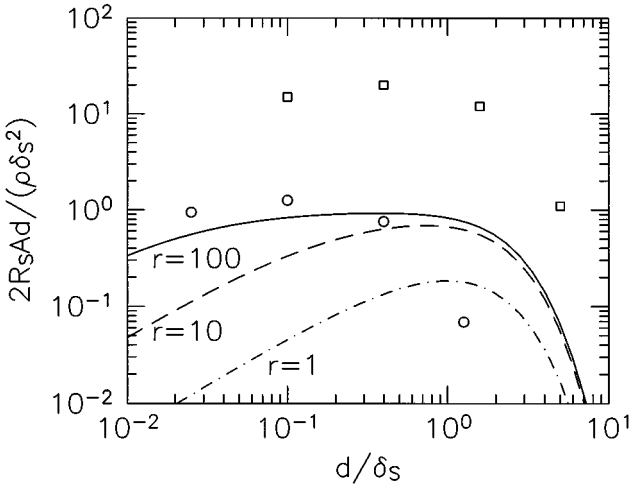

FIG. 3. The scaled spin-injection signal R_S vs the thickness of the film d. The curves are the theoretical result of Eq. (5.9) for different values of the dimensionless ratios $r_L=r_R=r$ of Eqs. (5.7) and (5.8) with $\eta_1'\eta_2'=1$. For d larger than the spin-diffusion length δ_S, the signal decays exponentially. For large junction resistance ($r=100$), the product $R_S d$ is roughly constant for a wide range of $d<\delta_S$, while for smaller junction resistances ($r=10$ or $r=1$), $R_S d$ decays more rapidly. Even for large junction resistance, $R_S d$ does eventually decay for small d. The points are from the experiment of Ref. 12 for the case where Permalloy is the ferromagnet. In plotting the data we have used two different values for the spin-diffusion length: $\delta_S=1\ \mu$m (squares) and $\delta_S=4\ \mu$m (circles). As explained in Ref. 12 if one adjusts δ_S to fit the falloff at large d, then the signal is larger than the theory, and if one adjusts δ_S to fit the small d data, then the experiment decays more quickly than the theory at large d. The resistivity of the paramagnet P is ρ, and $\mathcal{A}$ is the cross-sectional area of the current probe in Fig. 2.

In the same figure we have also plotted the data of Ref. 12 with Permalloy as the ferromagnet and gold as the paramagnet. Since the plot in Fig. 3 is scaled by the diffusion length in both the abscissa and ordinate, we have chosen two different diffusion lengths in plotting the data: $\delta_S=1\ \mu$m (squares) and $\delta_S=4\ \mu$m (circles). The 1 μm spin-diffusion length correctly describes the decay of the signal at large d, but produces too large a signal at small d. The 4 μm spin-diffusion length produces agreement at small d, but decays too rapidly at large d. Thus, it is not possible to fit the data quantitatively with this theory for all d, even though the length dependence of the data looks qualitatively similar to the theoretical curve for large junction resistance.

VI. CONCLUSION

In this paper we have used a two-component drift-diffusion equation for spin-up and spin-down electrons to compute the signal for recent spin-injection experiments. The length dependence of the signal is determined by the ratio of two resistances. The first resistance is the resistance

of the junctions between the ferromagnets and the paramagnet. The second resistance is determined by how quickly the magnetization relaxes in the metals. This resistance is larger for long spin-relaxation times.

When the junction resistances are large, we reproduce the results of Johnson and Silsbee: the spin-injection signal R_S decays exponentially for large sample thicknesses d, and is proportional to $1/d$ for sample thicknesses less than the spin-diffusion length. However, for sufficiently small sample thicknesses we do find that the signal eventually saturates. This saturation is due to the leakage of nonequilibrium magnetization out of the paramagnet into the current and voltage probes. For smaller junction resistances the size of the signal is smaller and the saturation of the $1/d$ behavior occurs for larger d. Thus, to enhance the spin-injection signal for thin samples one should use a large junction resistance.

The theory does fit qualitatively the length dependence of the data assuming large junction resistances. This includes a possible beginning of the saturation of the $1/d$ behavior for the smallest sample thickness measured. However, as with earlier analyses, it is not possible to quantitatively fit both the small d and large d data with the theory.

ACKNOWLEDGMENTS

The authors would like to thank Mark Johnson and Fred Sharifi for useful discussions. This work is supported by NSF Grant No. DMR-9357474, the NHMFL, and DOD/AFOSR Grant No. F49620-96-1-0026.

APPENDIX: ONSAGER RELATIONS

In this appendix we provide an alternate derivation of the results of Secs. IV and V for the signal R_S. This approach has the advantage that the current flow is very nearly one dimensional, and hence the reduction to and interpretation of our effective one-dimensional equation is more direct.

The Onsager relations for a resistance measurement applied to this problem state that the voltage measured is unchanged upon interchanging current and voltage probes.[17] Thus, the voltage measured by the probe configuration shown in Fig. 2(b) is the same as the voltage measured by the probe configuration in Fig. 2(c). This is a big advantage because the current flow in Fig. 2(c) does not change directions, but goes directly from left to right. There will be some fringing of the current flows in the paramagnetic region P; however, provided that the dimensions of the cross-sectional area $\mathcal{A}$ are large compared to the thickness of the paramagnetic regime, this fringing is small compared to the net current.

For the current flow shown in Fig. 2(c) we again derive effective one-dimensional equations and solve them. The solutions in the three regimes have the following form:

$$x<0:\frac{1}{j}\begin{pmatrix}V_\uparrow(x)\\ V_\downarrow(x)\end{pmatrix}=\begin{pmatrix}1\\1\end{pmatrix}\left\{\frac{-(x-x^L)}{\sigma_\uparrow^L+\sigma_\downarrow^L}\right\} \tag{A1}$$

$$+\begin{pmatrix}(\sigma_\uparrow^L)^{-1}\\ -(\sigma_\downarrow^L)^{-1}\end{pmatrix}\left\{\frac{j^L}{2\lambda_S^L}e^{+\lambda_S^L x}\right\},$$

$$0<x<d:\frac{1}{j}\begin{pmatrix}\mu_\uparrow/(-e)\\ \mu_\downarrow/(-e)\end{pmatrix}=\begin{pmatrix}1\\1\end{pmatrix}\left\{\frac{-x}{\sigma_\uparrow^M+\sigma_\downarrow^M}+\frac{x^L}{\sigma_\uparrow^L+\sigma_\downarrow^L}-V^L\right\}$$

$$+\begin{pmatrix}(\sigma_\uparrow^M)^{-1}\\ -(\sigma_\downarrow^M)^{-1}\end{pmatrix}\left\{\frac{j^{M1}}{2\lambda_S^M}e^{-x/L_S^M}+\frac{j^{M2}}{2\lambda_S^M}e^{+\lambda_S^M(x-d)}\right\}, \tag{A2}$$

$$x>d:\frac{1}{j}\begin{pmatrix}\mu_\uparrow/(-e)\\ \mu_\downarrow/(-e)\end{pmatrix}=\begin{pmatrix}1\\1\end{pmatrix}\left\{\frac{-(x-d)}{\sigma_\uparrow^R+\sigma_\downarrow^R}-\frac{d}{\sigma_\uparrow^M+\sigma_\downarrow^M}+\frac{x^L}{\sigma_\uparrow^L+\sigma_\downarrow^L}-V^L-V^R\right\}$$

$$+\begin{pmatrix}(\sigma_\uparrow^R)^{-1}\\ -(\sigma_\downarrow^R)^{-1}\end{pmatrix}\left\{\frac{j^R}{2\lambda_S^R}e^{-\lambda_S^R(x-d)}\right\}. \tag{A3}$$

Matching boundary conditions, the continuity of the spin current gives

$$p^L-j^L=j^{M1}-j^{M2}e^{-\lambda d}, \tag{A4}$$

$$p^R+j^R=j^{M1}e^{-\lambda d}-j^{M2}, \tag{A5}$$

where p^L is p of Eq. (3.12) and p^R is the same with $L\leftrightarrow R$. The Landauer formula applied to the left and right junctions gives

$$1+p^L-j^L=G_\uparrow^L\left(\frac{2V^L}{j}+R_\uparrow^L j^L-R_\uparrow^M[j^{M1}+j^{M2}e^{-\lambda d}]\right), \tag{A6}$$

$$1-p^L+j^L=G_\downarrow^L\left(\frac{2V^L}{j}-R_\downarrow^L j^L+R_\downarrow^M[j^{M1}+j^{M2}e^{-\lambda d}]\right), \tag{A7}$$

$$1+p^R+j^R=G_\uparrow^R\left(\frac{2V^R}{j}+R_\uparrow^M[j^{M1}e^{-\lambda d}+j^{M2}]-R_\uparrow^R j^R\right), \tag{A8}$$

$$1-p^R-j^R=G_\downarrow^R\left(\frac{2V^R}{j}-R_\downarrow^M[j^{M1}e^{-\lambda d}+j^{M2}]+R_\downarrow^R j^R\right). \tag{A9}$$

As in Sec. V the voltage measured has several different contributions. The voltage drop between x^L and 0 is again

independent of the orientation of the ferromagnets. The voltage drop across the left interface has a contribution of $-V^L$. Although it is not clear where in the middle paramagnetic region the voltage probe measures the voltage, for any choice of position, $0<x<d$, the voltage measured by the average electrochemical potential is invariant under magnetization reversal [see Eq. (A2)]. Thus, in this case the voltage measured is just $-V^L$:

$$R_S=\left(\frac{-V^L}{j\mathcal{A}}\right)_I-\left(\frac{-V^L}{j\mathcal{A}}\right)_{II}. \tag{A10}$$

Upon solving Eqs. (A4)–(A9) for V^L and substituting into Eq. (A10), we obtain exactly the same result as Eq. (5.9). In this manner we can infer that the third term in Eq. (5.3) is indeed invariant under magnetization reversal.

*Present address: Department of Physics, University of California, Los Angeles, CA 90024.

[1] P. M. Tedrow and R. Meservey, Phys. Rev. Lett. **26**, 192 (1971); Phys. Rev. B **7**, 318 (1973).
[2] X. Hao, J. S. Moodera, and R. Meservey, Phys. Rev. B **42**, 8235 (1990).
[3] M. N. Baibich, J. M. Broto, A. Fert, F. Nguyen Van Dau, F. Petroff, P. Etienne, G. Creuzet, A. Friederich, and J. Chazelas, Phys. Rev. Lett. **61**, 2472 (1988).
[4] B. Dieny, V. S. Speriosu, S. Menin, S. S. P. Parkin, B. A. Gurney, P. Baumgart, and D. R. Wilhoit, J. Appl. Phys. **69**, 4774 (1991).
[5] R. E. Camley and J. Barnas, Phys. Rev. Lett. **63**, 664 (1989).
[6] P. M. Levy, S. Zhang, and A. Fert, Phys. Rev. Lett. **65**, 1643 (1990).
[7] L. M. Falicov, Phys. Today **45** (10), 46 (1992).
[8] M. Johnson and R. H. Silsbee, Phys. Rev. Lett. **55**, 1790 (1985); Phys. Rev. B **37**, 5326 (1988).
[9] M. Johnson and R. H. Silsbee, Phys. Rev. B **35**, 4959 (1987); **37**, 5312 (1988).
[10] A. G. Aronov, Pis'ma Zh. Eksp. Teor. Fiz. **24**, 37 (1976) [JETP Lett. **24**, 32 (1976)].
[11] R. H. Silsbee, Bull. Magn. Reson. **2**, 284 (1980).
[12] M. Johnson, Phys. Rev. Lett. **70**, 2142 (1993); Science **260**, 320 (1993).
[13] M. Johnson, Phys. Rev. Lett. **67**, 3594 (1991).
[14] T. Valet and A. Fert, Phys. Rev. B **48**, 7099 (1993).
[15] A. Fert (private communication).
[16] R. Landauer, Philos. Mag. **21**, 863 (1970); E. N. Economou and C. M. Soukoulis, Phys. Rev. Lett. **46**, 618 (1981); D. S. Fisher and P. A. Lee, Phys. Rev. B **23**, 6851 (1981).
[17] L. Onsager, Phys. Rev. **38**, 2265 (1931); For a recent discussion in the context of resistance measurements see M. Buttiker, Phys. Rev. Lett. **57**, 1761 (1986).